ACS Pharmacology & Translational Science

pubs.acs.org/ptsci

Article

Development of Ultrapure and Potent Tannic Acids as a Pan-coronal Antiviral Therapeutic

Published as part of the ACS Pharmacology & Translational Science virtual special issue "New Drug Modalities in Medicinal Chemistry, Pharmacology, and Translational Science".

Po-Chang Shih,[†] Yi-Wen Mao,[†] Jhe-Wei Hu,[†] Han-Yi Hsieh,[†] Tsai-Miao Shih,[†] Lu-Ping Lu,[†] Wei-Hua Chang,[†] Chan-Hui Huang,[†] Chia-Hung Lin,[†] Chih-Hung Lin, Peng Tan, Ya-Ching Yang, Ming-Hong Chien, Chen-Che Su, Cheng-Hsin Yeh, Pei-Yun Chuang, Tien-Lan Hsieh, Ching-Cheng Wang, Po-Shiuan Hsieh, Teh-Ying Chou, and Guochuan Emil Tsai*

Cite This: https://doi.org/10.1021/acsptsci.1c00264

Read Online

ACCESS | Metrics & More | Article Recommendations

ABSTRACT: The rampageous transmission of SARS-CoV-2 has been devastatingly impacting human life and public health since late 2019. The waves of pandemic events caused by distinct coronaviruses at present and over the past decades have prompted the need to develop broad-spectrum antiviral drugs against them. In this study, our Pentarlandir ultrapure and potent tannic acids (UPPTA) showed activities against two coronaviral strains, SARS-CoV-2 and HCoV-OC43, the earliest-known coronaviruses. The mode of inhibition of Pentarlandir UPPTA is likely to act on 3-chymotrypsin-like protease (3CLpro) to prevent viral replication, as supported by results of biochemical analysis, a 3CLpro assay, and a "gain-of-function" 3CLpro overexpressed cell-based method. Even in the 3CLpro overexpressed environment, Pentarlandir UPPTA remained its antiviral characteristic. Utilizing cell-based virucidal and cytotoxicity assays, the 50% effective concentrations (EC_{50}) and 50% cytotoxicity concentration (CC_{50}) of Pentarlandir UPPTA were determined to be ∼0.5 and 52.5 μM against SARS-CoV-2, while they were 1.3 and 205.9 μM against HCoV-OC43, respectively. In the pharmacokinetic studies, Pentarlandir UPPTA was distributable at a high level to the lung tissue with no accumulation in the body, although the distribution was affected by the food effect. With further investigation in toxicology, Pentarlandir UPPTA demonstrated an overall safe toxicology profile. Taking these findings together, Pentarlandir UPPTA is considered to be a safe and efficacious pancoronal antiviral drug candidate that has been advanced to clinical development.

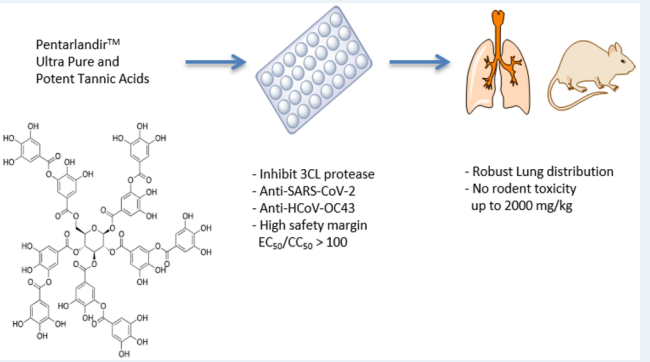

KEYWORDS: *SARS-CoV-2, 3-chymotrypsin-like protease, tannic acids, COVID-19, Pentarlandir*

A novel pneumonia identified in late 2019 from Wuhan, China, has been pandemic, impacting public health globally with disastrous morbidity and mortality. The virus causing this pneumonia has been isolated with a corona appearance observed under electron microscopy,[1] from which it was tentatively designated as 2019-nCoV. This coronavirus (CoV) was later formally named as severe acute respiratory syndrome coronavirus 2 (SARS-CoV-2), and the disease caused by it was called COVID-19.[2] The transmission of COVID-19 is rapid, with the number of confirmed cases reaching over 480 million globally as of April 2022, and with more transmissible and/or virulent mutants appearing over time.

In the wake of the highly pathogenic SARS-CoV-2 and its variants, the awareness of frequent CoV threats to humans has grown. Prior to SARS-CoV-2, major human CoVs included HCoV-OC43 (probable cause of the Russian flu in ∼1890),[3] HCoV-229E (1966), SARS-CoV (2002), HCoV-NL63 (2003), HCoV-HKU1 (2004), and MERS-CoV (2012), with the virus isolation year shown in parentheses.[4,5] These CoVs remain active in human populations, with varying degrees of impact. Such intermittent CoV emergence has aroused worry

Received: December 22, 2021

that many novel CoV strains/variants of concern will appear following SARS-CoV-2 which can cause severe or even catastrophic consequences. To lessen threats posed by current and future CoVs, developing pan-coronal antiviral drugs is therefore strongly recommended.[6]

The inhibition of viral replication has been thought to be an effective approach to preventing the morbidity and mortality of viral spread. For example, critical proteins involved in the life cycle of the SARS-CoV-2 have been characterized with known functions.[7] 3-Chymotrypsin-like protease (3CLpro), also known as the main protease and non-structural protein 5 (Nsp5), is responsible for the cleavages of the viral polyprotein to release Nsp4−16.[8] The functions of Nsp4−16 are to, for instance, unravel double-stranded DNA, modify RNA, cleave the polyprotein, and replicate the viral genome.[9] For all the variants of concern of SARS-CoV-2 identified so far, there is only one amino acid difference between the 3CLpro, K90R, of the β variant and the other one, P132H, of the o variant; for the variants of concern, G15S of λ and L205V of ζ were the only two. The limited genetic variations of 3CLpro suggest 3CLpro is a house-keeping gene of essential functioning that is an ideal drug target for developing pancoronal antiviral drugs. In addition, a substrate-binding pocket of the 3CLpro consisting of T25, L27, H41, M49, Y54, L141, N142, G143, S144, C145, H163, M165, E166, L167, P168, F185, Q189, T190, A191, Q192, and A193 has been concluded to be highly conserved among all CoVs following amino-acid sequence analysis too, where H41/C145 is the catalytic dyad critical for the proteolytic activity.[8,10] Accordingly, 3CLpro, specifically this binding site, could be a potential molecular target[11] to develop pan-coronal antiviral drugs.

Tannic acids are a group of naturally occurring polyphenol compounds with galloyl moieties expanded from a central glucose moiety and commonly seen ingredients in products such as tea,[12] wine,[13] and beer.[14] Tannic acids have a well-documented antioxidant property.[15,16] In addition, tannic acids have been found to be bioactive against cancers,[17] bacteria,[18,19] and, more intriguingly, viruses.[20] In 2005, Chen et al. reported that a tea extract containing tannic acids showed inhibitory activity against 3CLpro of SARS-CoV, with a half-maximal inhibitory concentration (IC_{50}) of 3 μM.[12] Later, amino-acid sequence analysis of 3CL proteases of SARS-CoV and SARS-CoV-2 demonstrated that the similarity between their amino acid sequences is 96%.[21] These results shed light on the potential of tannic acids for being developed as a drug candidate that could inhibit 3CLpro of SARS-CoV-2 and likely other CoV strains, acting as a pan-coronal antiviral drug.

In this study, we repurposed one of our investigational drug products (IP, product name: Pentarlandir). The IP has an active pharmaceutical ingredient (API) of tannic acids with a variety of numbers of galloyl moieties. The API was given the name of Pentarlandir ultrapure and potent tannic acids (UPPTA). Initially, we analyzed the sequence similarities of 3CLpro among some known CoV strains. Following that, we conducted molecular modeling to predict binding affinities and modes of Pentarlandir UPPTA, focusing on the substrate-binding site of SARS-CoV-2 3CLpro. Several cell-free assays were then applied to understand the binding of Pentarlandir UPPTA to 3CLpro, such as native gel electrophoresis, a 3CLpro enzymatic assay, and high-performance liquid chromatography (HPLC) analysis. A 3CLpro overexpressed cell line was applied to evaluate the 3CLpro inhibitory effect of Pentarlandir UPPTA *in cellulo*. The cytotoxicity and virucidal activities of Pentarlandir UPPTA were evaluated using a CCK8-based methodology and antiviral assays against two distinct CoVs. Subsequently, pharmacokinetic (PK) and toxicology studies were conducted to develop drug candidate profiles, ensuring the safety of the API.

RESULTS

Similarity Analyses of Amino Acid Sequences of 3CLpro from Distinct Coronavirus Strains. As mentioned above, the substrate binding site of 3CLpro was highly conserved among CoVs. We therefore examined the similarities of whole amino acid sequences among 3CLpro of some known CoVs, including SARS-CoV, MERS-CoV, HCoV-HKU1, HCoV-OC43, HCoV-NL63, and HCoV-229E (Figure 1). The alignment results indicated that 3CLpro is a conserved proteolytic protein for the CoVs, showing potential as a target for developing pancoronal antiviral drugs.

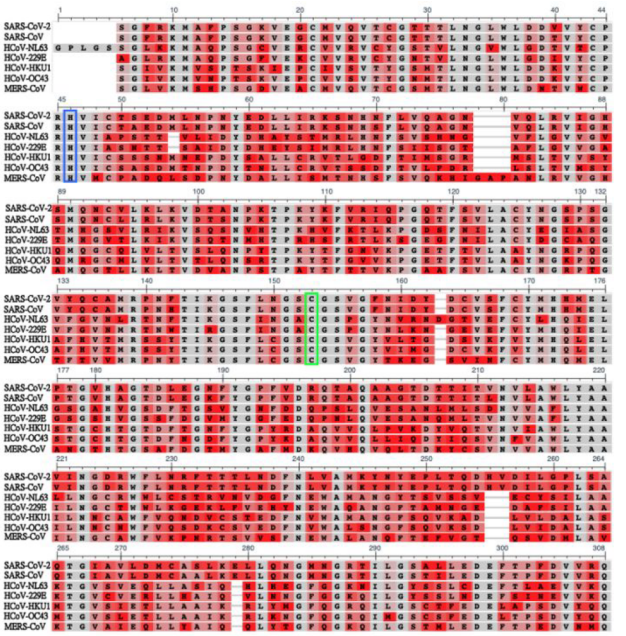

Figure 1. Alignment of the 3CLpro of human coronavirus strains. The consensus histidine and cysteine dyads are shown in blue and green frames, respectively. The amino acids with red shades have less consensus as compared to other gray residues at the same position. Following comparison with SARS-CoV-2, the high homologies in percentage are SARS-CoV, 96.1%; MERS-CoV, 50.7%; HCoV-HKU1, 49%; HCoV-OC43, 48.0%; HCoV-NL63, 44.3%; and HCoV-229E, 41.0%.

Molecular-Modeling-Aided Prediction of Binding Affinities and Modes of Pentarlandir UPPTA. In subsequent *in silico* simulations, 3CLpro of SARS-CoV-2 was selected for targeting with a focused pocket on its substrate binding site. Several species of tannic acids with confirmed chemical structures isolated from Pentarlandir UPPTA were applied for molecular modeling using DOCK 6 and a 3CLpro crystal structure of SARS-CoV-2 (PDB ID 6LU7). The substrate binding pocket was set as rigid, while the rotatable bonds of the tannic acids were set as flexible. Chemical names, their abbreviations, chemical structures, simulated binding affinities, and binding modes along with their Grid Scores and distances of hydrogen bonds are shown in Table 1. Our

https://doi.org/10.1021/acsptsci.1c00264
ACS Pharmacol. Transl. Sci. XXXX, XXX, XXX−XXX

Table 1. Molecular Modeling Results of Tannic Acids Focusing on the Substrate Binding Site of 3CLpro of SARS-CoV-2[a]

Chemical name/ Abbreviated name	Chemical structure	Binding mode	Grid Score (kcal/mol)	Number of H-bond	H-Bond (Å)
(2S,3R,4S,5R,6R)-3,4,5-tris(3,4-dihydroxy-5-(3,4,5-trihydroxybenzoyloxy)benzoyloxy)-6-((3,4-dihydroxy-5-(3,4,5-trihydroxybenzoyloxy)benzoyloxy)methyl)oxan-2-yl 3,4-dihydroxy-5-(3,4,5-trihydroxybenzoyloxy)benzoate/β-10G	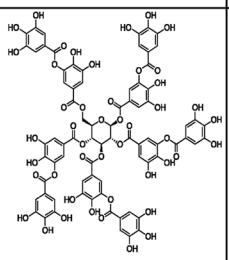	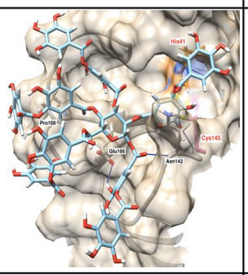	-82.89	5	Pro168 (2.5Å); Glu166 (2.6Å); Asn142 (2.5Å); **Cys145 (2.4Å); Cys145 (2.3Å)**
(2S,3R,4S,5R,6R)-3,4,5-tris(3,4,5-trihydroxybenzoyloxy)-6-((3,4,5-trihydroxybenzoyloxy)methyl)oxan-2-yl 3,4,5-trihydroxybenzoate/β-5G	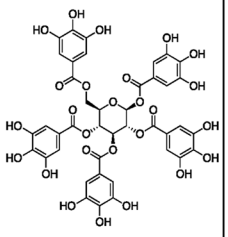	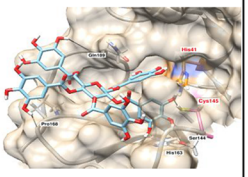	-73.19	5	Pro168 (2.4Å); Gln189 (2.3Å); His163 (2.1Å); Ser144 (2.2Å); **Cys145 (2.6Å)**
(2S,3R,4S,5R,6R)-4-(3,4-dihydroxy-5-(3,4,5-trihydroxybenzoyloxy) benzoyloxy)-5-hydroxy-3-(3,4,5-trihydroxybenzoyloxy)-6-((3,4,5-trihydroxybenzoyloxy)methyl)oxan-2-yl 3,4,5-trihydroxybenzoate/β-5G_m	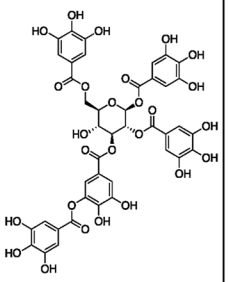	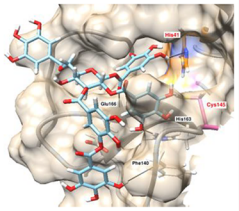	-75.44	5	Glu166 (2.0Å); Phe140 (2.5Å); His163 (2.4Å); **Cys145 (2.1Å); His41 (2.3Å)**
(2S,3R,4S,5R,6R)-4-(3,5-dihydroxy-4-(3,4,5-trihydroxybenzoyloxy) benzoyloxy)-5-hydroxy-3-(3,4,5-trihydroxybenzoyloxy)-6-((3,4,5-trihydroxybenzoyloxy)methyl)oxan-2-yl 3,4,5-trihydroxybenzoate/β-5G_p	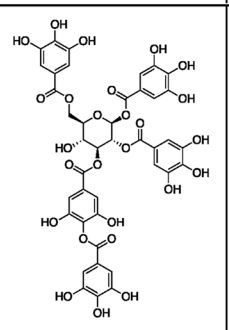	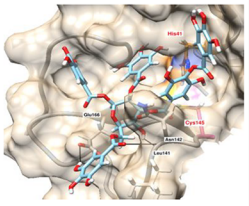	-84.01	4	Glu166 (2.3Å); Leu141 (2.7Å); Asn142 (2.5Å); **Cys145 (2.2Å)**
(2S,3R,4S,5R,6R)-4-(3,5-dihydroxy-4-(3,4,5-trihydroxybenzoyloxy) benzoyloxy)-3,5-bis(3,4,5-trihydroxybenzoyloxy)-6-((3,4,5-trihydroxybenzoyloxy)methyl)oxan-2-yl 3,4,5-trihydroxybenzoate/β-6G_p	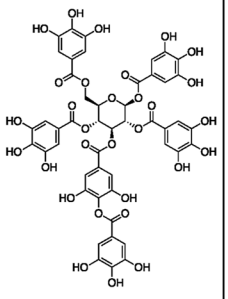	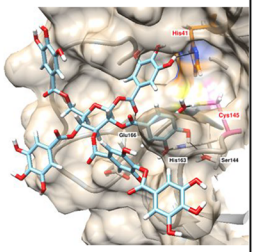	-81.79	5	Glu166 (2.0Å); His163 (2.2Å); Ser144 (2.2Å); **Cys145 (2.6Å); His41 (2.5Å)**

[a]The binding modes of the tannic acids are presented as balls and sticks, while the binding site is shown as space filling in gray. The H-bonds between molecules are presented as black lines. Key residues of the binding site are labeled in bold.

https://doi.org/10.1021/acsptsci.1c00264
ACS Pharmacol. Transl. Sci. XXXX, XXX, XXX−XXX

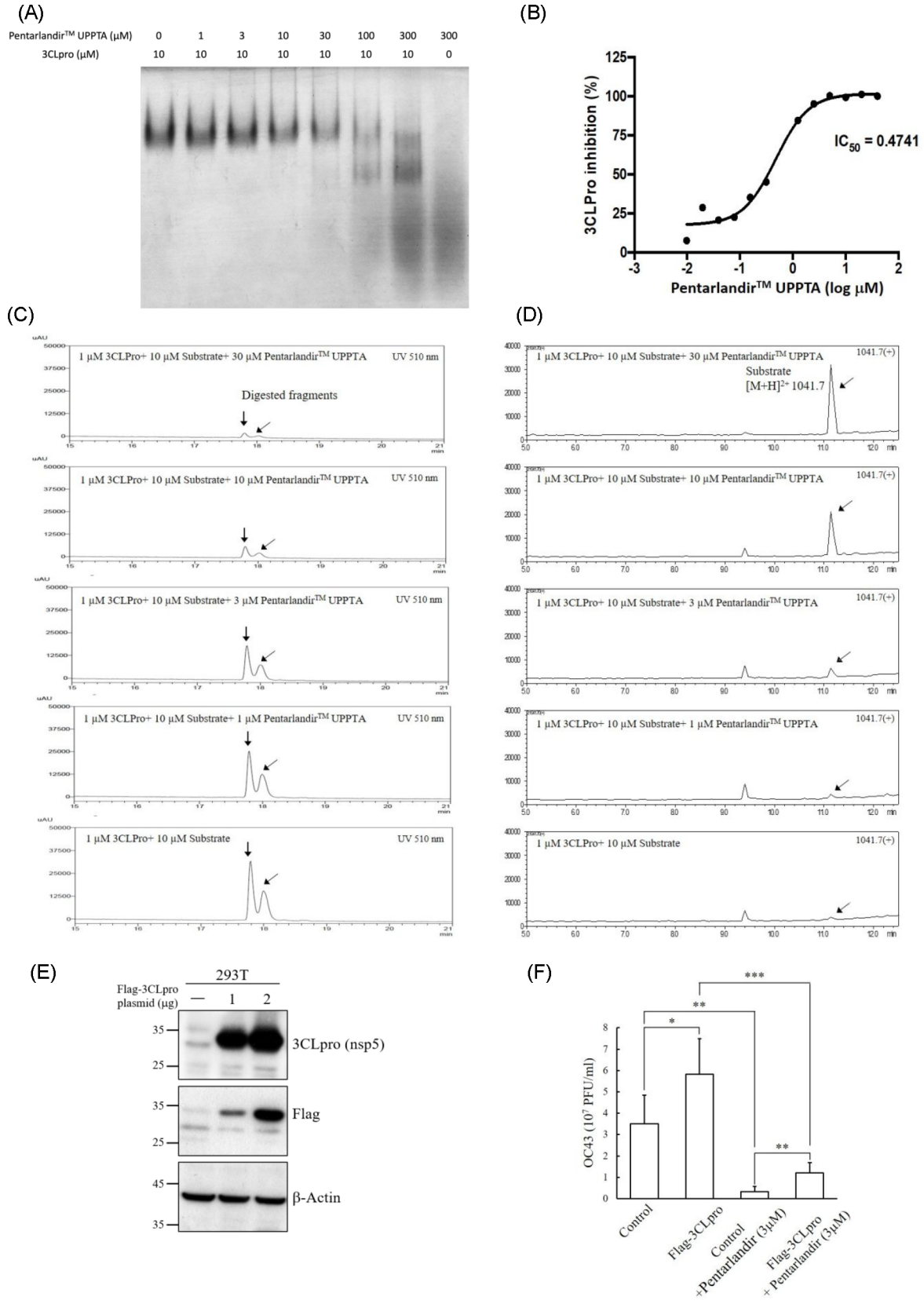

Figure 2. Evaluation of the inhibitory activity of Pentarlandir UPPTA on the 3CLpro. (A) Native gel electrophoresis of Pentarlandir UPPTA on the 3CLpro. (B) The IC_{50} of Pentarlandir UPPTA was determined to be 0.474 μM. (C, D) 3CLpro proteolytic activity (1 μM) to the 3CLpro-specific peptide substrate (10 μM) was ablated by Pentarlandir UPPTA (1−30 μM) in a dose-dependent manner following HPLC-PDA-MS analysis. (E) Western blot gel showing overexpressed Flag-3CLpro in 293T cells. (F) Using HCoV-OC43 as the infection virus, treatment with Pentarlandir UPPTA yielded lower PFU in both the control and Flag-3CLpro-overexpressed 293T cells.

https://doi.org/10.1021/acsptsci.1c00264
ACS Pharmacol. Transl. Sci. XXXX, XXX, XXX−XXX

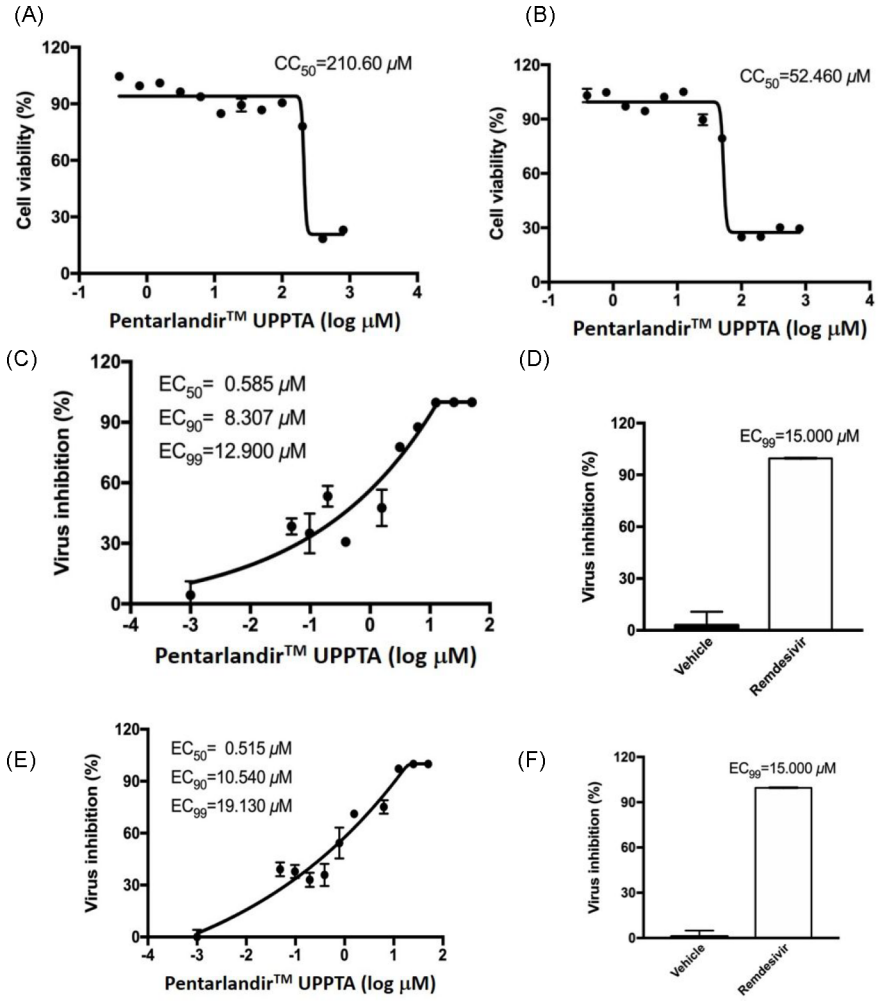

Figure 3. Cytotoxicity and antiviral activity of Pentarlandir UPPTA against SARS-CoV-2 in Vero E6 cells. (A) The CC_{50} of Pentarlandir UPPTA (using ddH_2O as the vehicle) was 210.60 μM following 24 h incubation in DMEM supplemented with 10% FBS. (B) The CC_{50} of Pentarlandir UPPTA (using DMSO as the vehicle) in DMEM supplemented with 2% FBS was determined to be 52.46 μM after 24 h. The final concentration of the DMSO in the culture medium was 1% (v/v). (C) The EC_{50}, EC_{90}, and EC_{99} of Pentarlandir UPPTA were 0.585, 8.307, and 12.90 μM, respectively, determined from the supernatant. (D) The EC_{99} of remdesivir was 15.00 μM from the supernatant of Vero E6 cells. (E) The respective EC_{50}, EC_{90}, and EC_{99} of Pentarlandir UPPTA were 0.515, 10.54, and 19.13 μM following the analyses of the cells. (F) The EC_{99} of remdesivir was 15.00 μM from the cell.

findings predicted strong affinities of the multiple species of UPPTA with 3CLpro of SARS-CoV-2.

The Mechanism of Inhibition of Pentarlandir UPPTA Could Be on the 3CLpro of Coronaviruses. Following the computational predictions, the inhibitory property of Pentarlandir UPPTA on SARS-CoV-2 3CLpro enzymatic activity was further evaluated using the native gel electrophoresis, the 3CL protease assay, and confirmation of the inhibition of the protease cleavage by HPLC. As shown on the native gel, when the 3CLpro was alone, the protein band was aggregated with limited shift, while Pentarlandir UPPTA itself demonstrated smearing bands. When different concentrations of Pentarlandir UPPTA were mixed with a fixed concentration of the 3CLpro, the smearing effect was found to be concentration-dependent, indicating that Pentarlandir UPPTA could bind to the 3CLpro (Figure 2A). In the 3CL protease assay, a fluorescent 3CLpro-specific peptide substrate, containing the cleavage site of Nsp4/5 at Gln-Ser, was used as a probe, incubating with the 3CLpro and Pentarlandir UPPTA. Our findings demonstrated a potent inhibition of Pentarlandir UPPTA on the 3CLpro, with IC_{50} determined to be 0.474 μM, much more potent than the crude tannic acid (Figure 2B).[12] Prior to HPLC-PDA-MS analysis, the 3CLpro and a 3CLpro-specific peptide substrate were incubated with or without Pentarlandir UPPTA. The results showed that Pentarlandir UPPTA was able to ablate the signal intensity of 3CLpro-hydrolyzed peptide fragments, while the signal intensity of the peptide substrate was increased, indicating that the hydrolytic activity of 3CLpro was dose-dependently inhibited (Figure 2C,D). Following the display of Pentarlandir UPPTA's activity against the 3CLpro in the cell-free assays, its potential mechanism of inhibition *in cellulo* was tested in a 3CLpro-overexpressed cellular system. A 293T cell line was transfected with a plasmid containing sequences of Flag-tagged 3CLpro of SARS-CoV-2 to yield a 3CLpro-overexpressed cell line. The success of Flag-3CLpro transfection was validated using Western blot analysis in which primary antibodies against 3CLpro and Flag were able to detect the presence of Flag-3CLpro in cell lysates. The amount of 3CLpro was clearly increased in 293T cells transfected with Flag-3CLpro-containing plasmid, compared with the control (Figure 2E). Using HCoV-OC43 as the infection virus, we found the viral plague formation unit (PFU) was much higher

https://doi.org/10.1021/acsptsci.1c00264
ACS Pharmacol. Transl. Sci. XXXX, XXX, XXX−XXX

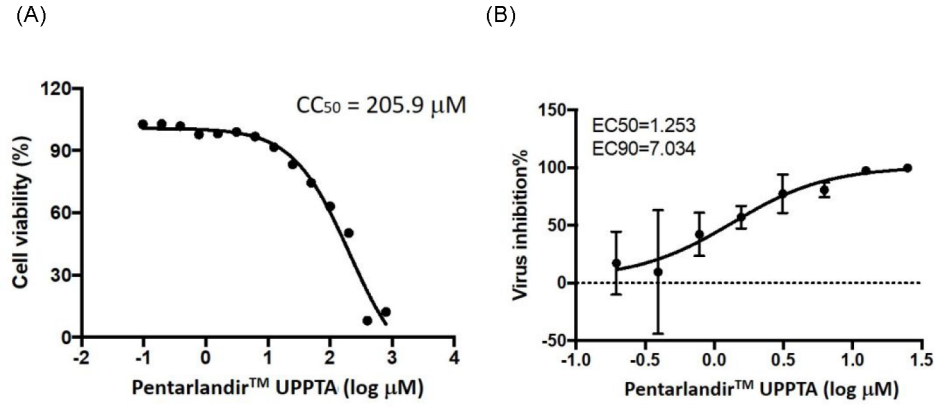

Figure 4. Cytotoxicity and antiviral activity of Pentarlandir UPPTA against HCoV-OC43 in HCT8 cells. (A) The CC_{50} of Pentarlandir UPPTA was 205.9 μM. (B) The respective EC_{50} and EC_{90} of Pentarlandir UPPTA were 1.253 and 7.034 μM following the analyses of the cell layer.

Table 2. Average Pharmacokinetic Parameters of Pentarlandir UPPTA in Plasma in Each Animal Group

condition/dosage	T_{max} (h)	C_{max}(μM)	$T_{1/2}$ (h)	$AUC_{0\text{-}t}$ (μM·h)	$AUC_{0\text{-}\infty}$ (μM·h)
fed, single dose/1000 mg/kg	3.40 ± 1.82	0.91 ± 0.35	3.90 ± 2.23	4.84 ± 1.92	6.73 ± 2.91
fasting, single dose/350 mg/kg	5.33 ± 0.82	0.69 ± 0.57	3.48 ± 2.44	2.39 ± 1.31	4.10 ± 1.73
fasting, single dose/750 mg/kg	2.60 ± 1.82	2.12 ± 0.65	2.58 ± 1.17	13.82 ± 7.61	13.94 ± 7.65
fasting, single dose/1000 mg/kg	3.71 ± 1.60	4.59 ± 1.36	2.74 ± 1.63	26.06 ± 9.58	30.16 ± 13.24
fasting, 14-day repeated dose/1000 mg/kg/day	4.83 ± 0.98	3.62 ± 1.74	6.01 ± 0.78	34.13 ± 11.39	36.73 ± 12.20

in the Flag-3CLpro-overexpressed than the control, indicating that 3CLpro is critical in significantly increasing the viral load. This suggested a gain-of-function-like phenomenon by overexpressing 3CLpro. However, after treatment with Pentarlandir UPPTA, both cell lines showed significant decreases in the PFUs. This implied that Pentarlandir UPPTA retains its antiviral characteristic even in an 3CLpro-overexpressed environment (Figure 2F). Collectively, all the above findings suggest that 3CLpro is likely a target for Pentarlandir UPPTA.

Cytotoxicity and Virucidal Effects of Pentarlandir UPPTA. Once it was confirmed that Pentarlandir UPPTA could work against the CoV *in cellulo*, the cytotoxicity and virucidal effects of Pentarlandir UPPTA were subsequently evaluated in cells against SARS-CoV-2 and HCoV-OC43 strains. For SARS-CoV-2, CCK8-based methodology was applied to test cytotoxicity using Vero E6 cells; either distilled, deionized water (ddH_2O) or dimethylsulfoxide (DMSO) was used as the vehicle. In the ddH_2O vehicle group, the 50% cytotoxicity concentration (CC_{50}) of Pentarlandir UPPTA was determined to be 210.60 μM after 24 h with the cells maintained in Dulbecco's modified Eagle medium (DMEM) and 10% fetal bovine serum (FBS) (Figure 3A). In the DMSO vehicle group, the CC_{50} of Pentarlandir UPPTA in DMEM supplemented with 2% FBS was determined to be 52.46 μM after 24 h (Figure 3B). On the other hand, in the virucidal assay, SARS-CoV-2-containing medium with a multiplicity of infection (MOI) of 0.01 was added to Pentarlandir UPPTA-containing wells seeded with Vero E6 cells. Our findings showed that the effective concentrations (EC_{50}, EC_{90}, and EC_{99}) determined from the supernatant were 0.585, 8.307, and 12.900 μM, respectively (Figure 3C). In comparison, remdesivir exhibited EC_{99} at 15.00 μM in the supernatant under the same experimental conditions (Figure 3D). On the other hand, the EC_{50}, EC_{90}, and EC_{99} determined from the cell layer were 0.515, 10.540, and 19.130 μM, respectively (Figure 3E). In comparison, remdesivir exhibited EC_{99} at 15.00 μM in the cell layer under identical experimental conditions (Figure 3F).

For the HCoV-OC43 arm, HCT8 cells were used, and the procedures of cytotoxicity and virucidal assays were modified from the assays for SARS-CoV-2. The cytotoxicity findings demonstrated that the CC_{50} of Pentarlandir UPPTA was 205.9 μM (using DMSO as the vehicle) following 24 h incubation in RPMI medium supplemented with 2% FBS. The final concentration of the DMSO in the culture media was 0.5% (v/v) (Figure 4A). In the virucidal assay, the EC_{50} and EC_{90} of Pentarlandir UPPTA were determined to be 1.253 and 7.034 μM, respectively, following the analyses of the cell layer (Figure 4B).

Pharmacokinetics of Pentarlandir UPPTA. The PK studies to investigate the absorption profile of Pentarlandir UPPTA were conducted in male Sprague−Dawley rats via oral gavage. The rats received a single dose of 1000 mg/kg under a fed condition. Blood samples were collected to analyze the area under the concentration−time curve from time 0 to the last sampling time or infinite time ($AUC_{0\text{-}t}$ or $AUC_{0\text{-}\infty}$), maximum plasma concentration (C_{max}), the time to reach C_{max} (T_{max}), and half-life ($T_{1/2}$).

We next investigated two aspects: whether food would affect absorption of the drug candidate, and whether the absorption was proportional to increasing dosage levels. Accordingly, rats were randomly assigned to receive a single dose of 350, 750, or 1000 mg/kg under a fasting condition. Our findings showed that C_{max} and $AUC_{0\text{-}t}$ were in proportion to the administered dosage levels (coefficient of determination R^2 = 0.92 for C_{max} and 0.98 for $AUC_{0\text{-}t}$), and Pentarlandir UPPTA was significantly impacted by the food effect ($p < 0.01$).

Based on these findings, a dose of 1000 mg/kg under the fasting condition was selected for a subsequent 14-day repeat-dose PK study to further understand drug accumulative effects. In comparison with the single-dose study of 1000 mg/kg under the fasting condition, the results of the 14-day repeat-dose PK study showed that 14-day administration led to an insignificant

https://doi.org/10.1021/acsptsci.1c00264
ACS Pharmacol. Transl. Sci. XXXX, XXX, XXX−XXX

increase in AUC_{0-t} (26.06 ± 9.58 versus 34.13 ± 11.39 μM·h, respectively, p = 0.19), while C_{max} did not increase as anticipated (4.59 ± 1.36 versus 3.62 ± 1.74 μM, respectively), as shown in Table 2. Collectively, these findings suggest that Pentarlandir UPPTA is affected by the food effect, and it would not accumulate.

Since it is known that SARS-CoV-2 affects patients' lungs in particular, we next investigated the lung distribution of Pentarlandir UPPTA in male Sprague−Dawley rats. The drug concentration was measured in the lung tissue within 24 h after single-dose or 14-day oral administration in rats at 1000 mg/kg/day under the fasting condition. The concentration−time results demonstrated that the concentration of Pentarlandir UPPTA was the highest at 4−7 and 4 h in the single-dose and 14-day repeat-dose studies, respectively. The 14-day repeated dosing of Pentarlandir UPPTA did not contribute to drug accumulation in lungs (Table 3). Taken together, the results suggest that Pentarlandir UPPTA could reach the highest concentration in the lungs as early as 4 h, whereas it did not accumulate in the lung.

Table 3. Concentrations of Pentarlandir UPPTA in Lung

group	duration	collection time (h)	average (μg/g lung)
1	single dose	4	0.70 ± 0.41
2		7	1.06 ± 1.03
3		24	0.57 ± 0.16
4	14-day repeat dose	4	1.57 ± 1.55
5		7	0.90 ± 0.68
6		24	1.01 ± 1.12

An additional study was carried out to determine the highest dose that would reach saturation in plasma concentrations (C_{max} and AUC_{0-t}) of male Sprague−Dawley rats. Since Pentarlandir UPPTA would not accumulate in the rodent body, a single dose study was performed with dosage levels of 800, 1600, 2000, and 2400 mg/kg orally administered to rats. Our findings demonstrated that the saturation dose was determined to be above 2000 mg/kg (Figure 5).

Toxicology of Pentarlandir UPPTA. Our PK findings showed that doses above 2000 mg/kg of Pentarlandir UPPTA reached saturation in rats, and therefore, we conducted a toxicological study with the highest oral dose peaking at 2000 mg/kg. Three doses at 800, 1600, and 2000 mg/kg/day were selected for the subsequent 14-day repeat-dose toxicity study in male and female rats. The rats were randomly assigned to receive one of the doses per day via oral gavage for 14 consecutive days, followed by an additional 14-day recovery period (i.e., no drug administered) to observe any delayed onset of toxicity, persistence, or reversibility.

A full panel of toxicology endpoints was collected, including clinical signs, body weight, food consumption, hematology, coagulation, clinical biochemistry, ophthalmic examination, organ weights, and macroscopic and microscopic evaluation of a full panel of organs and tissues. Our results showed no clinical signs of toxicity, mortality, and ophthalmologic abnormality throughout the entire study period, except for a few small transitory changes, in all the dosage groups.

Mild changes in alanine transaminase (ALT) and Total Protein were noted in both genders in the 2000 mg/kg group, but they were all normalized by the end of the recovery period. Small decreases in body weight were noted among male rats in the two higher-dose groups, but they were all restored by the end of the recovery period. No significant changes in food consumption were noted, and no toxicity evidence was noted in the gross observation.

In histopathology evaluation, minimal bile duct hyperplasia was observed in both genders in the 1600 and 2000 mg/kg groups, which showed no progression by the end of the recovery period. Mild mononuclear cell infiltration was observed in one animal in both genders in the 2000 mg/kg group, which was also improved to the minimal level at the end of the recovery period. The mild temporary changes were not accompanied by other indicators of hepatobiliary pathology, such as elevation in total bilirubin, alkaline phosphatase, aspartate aminotransferase, or γ-glutamyl transferase levels. From the findings, the no-observed-adverse-effect level (NOAEL) dose was estimated to be 2000 mg/kg. Overall, our results suggest that Pentarlandir UPPTA is safe for use up to 2000 mg/kg in rats, of which the dosage level matches a human equivalent dose (HED) of 322.6 mg/kg.

DISCUSSION

We have screened drug candidates from our chemical library to develop a chemotherapeutic treatment for CoV-induced diseases such as COVID-19. Through the protease assay and the rest methods, we endeavored to repurpose Pentarlandir UPPTA. Supported by the overexpression study showing that Pentarlandir UPPTA is still effectively virucidal when the viral activity is significantly enhanced, we concluded that one mechanism of inhibition of Pentarlandir UPPTA is to target 3CLpro of SARS-CoV-2. Suggested by the high similarity in amino acid sequences of 3CLpro, Pentarlandir UPPTA showed potential to inhibit other CoVs, which has been validated using the cellular assays. Pentarlandir UPPTA demonstrated

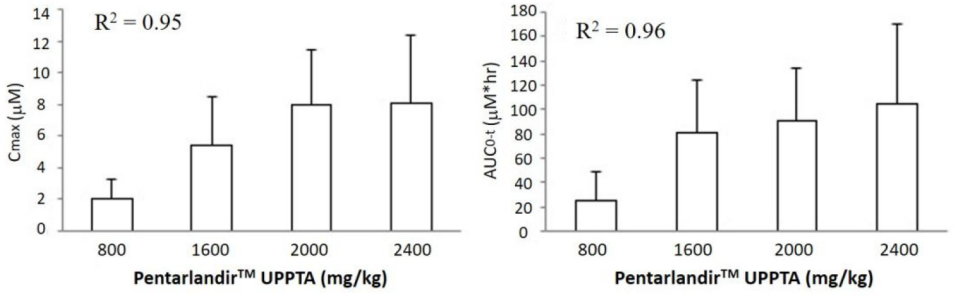

Figure 5. Plasma concentrations of Pentarlandir UPPTA in male rats administered with 800, 1600, 2000, or 2400 mg/kg. (A) The C_{max}, R^2 = 0.95. (B) The AUC_{0-t}, R^2 = 0.96.

https://doi.org/10.1021/acsptsci.1c00264
ACS Pharmacol. Transl. Sci. XXXX, XXX, XXX−XXX

inhibitory activities against SARS-CoV-2 with $CC_{50} \approx 52$ μM and $EC_{50} \approx 0.5$ μM in Vero E6 cells, while it acted against HCoV-OC43 with $CC_{50} \approx 206$ μM and $EC_{50} \approx 1.3$ μM in HCT8 cells. Intriguingly, Wang et al. reported that tannic acids also inhibited TMPRSS2,[25] a cell surface protein critical for viral entry into human cells, strongly indicating dual protease targets of Pentarlandir UPPTA (i.e., 3CLpro and TMPRSS2) when developed to be a COVID-19 treatment.

In comparison with other anti-SARS-CoV-2 drug candidates, cellular assay-determined parameters demonstrated the advantages of Pentarlandir UPPTA in terms of virucidal activity, albeit assay conditions may not be identical. The IC_{50} values determined for lopinavir, saquinavir, nelfinavir, and tipranavir by Vatansever et al. were 486, 411, 234, and 180 μM, respectively, whereas ritonavir failed to inhibit 3CLpro at 20 μM.[26] Clearly, Pentarlandir UPPTA is at least 300-fold more active against 3CLpro than these antiviral drugs. On the other hand, the EC_{50} values determined for lopinavir, ritonavir, and remdesivir by Choy et al. were 26.10, >100, and 26.90 μM, respectively, while their CC_{50} values were 49.75, 48.91, and >100 μM, respectively.[23] Likewise, Pentarlandir UPPTA demonstrates stronger potency than the antiviral therapeutics *in cellulo*. Besides, after calculating their therapeutic indices, Pentarlandir UPPTA shows a wider therapeutic window (~100, 1.91, <0.489, and >3.72 for Pentarlandir UPPTA, lopinavir, ritonavir, and remdesivir, respectively).

Table 2 could help predict whether the PK concentration of Pentarlandir UPPTA would achieve the desired antiviral effects against SARS-CoV-2 in rats. As shown Table 2, all the C_{max} values are substantially higher than the $EC_{50} \approx 0.5$ μM evaluated in the SARS-CoV-2 virucidal study, strongly suggesting that Pentarlandir UPPTA could effectively inhibit SARS-CoV-2 activity *in vivo*.

Overall, our findings indicate that Pentarlandir UPPTA is safe and efficacious. Since Janower et al. reported potential hepatotoxicity caused by tannic acids,[27] we have carefully assessed the safety of Pentarlandir UPPTA *in vivo* under good laboratory practice (GLP) regulations. In the report by Janower et al., tannic acids were added for use as a colonic evacuation enhancer in barium enemas, with a few cases of liver toxicity reported after barium enema examinations. Such liver failure was presumed to be secondary to tannic acids and/or the performance of barium enemas.[27] We have conducted the 14-day repeat-dose toxicity study under GLP regulations, evaluating a full panel of toxicology endpoints. Our findings showed that the drug candidate had no significant abnormalities in any organs, biochemistry parameters, and other evaluations. The NOAEL value was above 2000 mg/day, which has a HED of 322 mg/kg, endorsing the safe use of Pentarlandir UPPTA. The reasons why tannic acids were associated with liver toxicity in the report of Janower et al. are clarified as follows. The extraction methods used at the time were not as sophisticated as ours, leading to an undetermined state of purity and composition. In contrast, Pentarlandir UPPTA utilized a proprietary modern technology developed to execute extraction, with a unique composition, and manufactured under current good manufacturing practice (cGMP), ensuring that the contents are controlled and consistent throughout the entire production process.

Taken together, Pentarlandir UPPTA, as a group of polyphenol structures with galloyl moieties extending from a central glucose moiety, demonstrates a safe and efficacious profile, showing great potential to serve as a lead in the development of pancoronal antiviral treatments. This investigational drug is currently undergoing clinical development (NCT04911777).

While this manuscript was in preparation, another inhibitor of 3CLpro, nirmatrelvir [PF-07321332],[28] which is part of Paxlovid, was granted emergency use by the U.S. FDA authorization for patients infected with SARS-CoV-2 and carrying high risk of progression. We consider, similar to other retroviruses, that protease inhibitors will become a major class of therapeutics for the treatment of coronavirus infections.

MATERIALS AND METHODS

API Preparation. The crude tannic acids from the natural source of Chinese tannic acids were subjected to a proprietary processing for API manufacturing and experimentation. The tannic acid purity in Pentarlandir UPPTA, manufactured under cGMP, was determined to be 98.6%, in comparison with a 99.4% reference standard.

Similarity Analysis of Amino Acid Sequences of 3CL Proteases. NCBI reference sequences used in the alignment were as follows: SARS-CoV-2, YP_009742612.1; SARS-CoV, NP_828863; MERS-CoV, YP_009047233.1; HCoV-NL-63, 5GWY_B; HCoV-229E, 2ZU2_B; HCoV-OC43, YP_009555250; and HCoV-HKU1, YP_459936.1. The sequences were subjected to a web version of constraint-based alignment tool (COBALT) on the National Center for Biotechnology Information (NCBI) Web site for analysis.

Molecular Modeling. The crystal structure of 3CLpro was modified from the complex with PDB ID 6LU7, which contains 3CLpro in complex with a small-molecule inhibitor, N3. The inhibitor N3 and water molecules were removed using Chimera 1.12 prior to the docking run. Dock 6 was utilized for ligand−protein complex simulations. The docked tannic acid molecules were the components isolated from Pentarlandir UPPTA. The stereo conformations of the tannic acids were energy minimized by Avogadro version 1.2 using the MMFF94 force field and other algorithms with default setting, and the grid generation was conducted following the Rizzo Lab tutorial (2018 DOCK tutorial 1 with PDB ID 2NNQ) with its default setting. Top-ranking binding modes and Grid Scores were selected and visualized using UCSF Chimera version 1.12.

Native Polyacrylamide Gel Electrophoresis. Recombinant SARS-CoV-2 3CL protease (10 μM) incubated with ascendant concentrations of Pentarlandir UPPTA from 1 to 300 μM was shaken at 99 rpm by program 61 (RM-2L Intellimixer, ELMI Ltd.) at 4 °C for 3 h. The reaction mixture, 3CL protease (10 μM), and Pentarlandir were mixed with sample buffer (5×) containing 62.5 mM Tris-HCl (pH 6.8), 25% glycerol, and 1% bromophenol blue, respectively. All samples were subjected to native polyacrylamide gel that did not contain sodium dodecyl sulfate at 80 V and 4 °C for 100 min. The gel was stained with Coomassie R-250 Brilliant Blue dye and then destained by deionized water until the background of the gel was fully destained.

Expression and Purification of 3CLpro. The experimental procedures of 3CLpro expression and purification were modified from the literature.[22] For protein expression, the amplified complementary DNA product containing viral 3CLpro genome linked with a glutathione S-transferase tag was inserted into a pET42b vector. Subsequently, the pET42b vector was transformed into *Escherichia coli* strain BL21. The transformed bacteria cells with pET42b-3CLPro were incubated on Luria−Bertani (LB) agar plates with 100 μg/

https://doi.org/10.1021/acsptsci.1c00264
ACS Pharmacol. Transl. Sci. XXXX, XXX, XXX−XXX

mL kanamycin for selection (37 °C; 14−16 h). Kanamycin-resistant clones were isolated and cultured in a 250 mL flask until they reached an optical density of 0.8 at 600 nm. Protein expression was induced with the addition of 0.4 mM isopropyl-β-D-1-thiogalactopyranoside (IPTG) at 16 °C. After 22 h, cultured cells were harvested by centrifugation and lysis. Finally, SARS-CoV-2 3CLpro was purified from bacterial lysates using a Glutathione Sepharose 4B column at 4 °C before being incubated with 1% Factor Xa protease solution to remove the glutathione S-transferase tag. The untagged 3CLpro was dialyzed in a buffer of 12 mM tris-(hydroxymethyl)aminomethane hydrochloride (Tris-HCl), 120 mM sodium chloride (NaCl), 0.1 mM ethylenediaminetetraacetic (EDTA), 20% glycerol, and 2 mM dithiothreitol (DTT), pH 7.4, before storage at −20 °C.

3CL Protease Assay. The experimental procedures of the 3CL protease assay were modified from the literature.[22] The fluorescent substrate (Genomics, Taiwan) was a 12-mer amino acid peptide (TSAVLQSGFRKM) with a Lys residue at the N-terminus and Glu at the C-terminus for the attachments of fluorophores 4-(4-dimethylaminophenylazo)benzoic acid (Dabcyl) and 5-[(2-aminoethyl)amino]naphthalene-1-sulfonic acid (Edans), respectively. The peptide substrate powder and Pentarlandir UPPTA were dissolved in sterile ddH_2O as a stock. The enzymatic assay was performed in 20 mM bis(2-hydroxyethyl)amino-tris(hydroxymethyl)methane (Bis-Tris), pH 7.4.

To carry out the assay, test article samples were added into each well of a 96-well plate, followed by the addition of 3CLpro. The 96-well plate was sealed and incubated at 37 °C for 30 min. Subsequently, the peptide substrate was added and mixed gently at 37 °C. Final concentrations of each assay component in a well were 50 nM 3CLpro, 6 μM peptide substrate, and various concentrations of the drug candidate. Each concentration of Pentarlandir UPPTA was evaluated in triplicate. The intensity of fluorescence signals was detected using a fluorescence microplate reader at 37 °C for 4 min. The excitation and emission wavelengths were 360 and 485 nm, respectively. The protease activity was presented as fluorescence intensity and calculated using the following equation: inhibition (%) = 1 − [(fluorescence sample, 4 min − fluorescence sample, 0 min)/(fluorescence ddH_2O, 4 min − fluorescence ddH_2O, 0 min)] × 100%.

HPLC-PDA-MS Analysis. Before being subjected to HPLC-PDA-MS analysis, the reaction mixture samples containing 3CLpro (1 μM), the substrate (10 μM), and Pentarlandir UPPTA were prepared identically to the 3CL protease assay. The chromatographic analysis was performed on a Shimadzu LCMS-2020 system (Shimadzu, Japan). A Kinetex XB-C18 column (5 μm, 150 mm × 4.6 mm i.d., Phenomenex, US) and a Phenomenex Luna C18 column (5 μm, 150 mm × 4.6 mm i.d., Phenomenex, US) were used for HPLC-PDA-MS analysis to detect fragments and substrate, respectively. A gradient mobile phase containing 0.1% trifluoroacetic acid mixed with increasing concentrations of acetonitrile was applied with a flow rate of 0.6 mL/min. A UV absorbance wavelength of 510 nm and the ESI-MS source set at positive ionization mode were applied to detect fragments and substrate signals, respectively.

Western Blotting Analysis. Cells were lysed in a modified RIPA buffer (50 mM Tris pH 8.0, 150 mM NaCl, 0.1% SDS, 1% NP-40, 1% Triton X-100, and 0.5% sodium deoxycholate with protease inhibitor and/or phosphatase inhibitor cocktail added immediately before use) on ice for 30 min and centrifuged at 13 000 rpm for 10 min. Protein samples were subjected to SDS-PAGE and transferred to PVDF membranes. The membranes were blocked with 5% bovine serum albumin and developed overnight using anti-SARS-CoV-2-3CLpro (Nsp5) (Cat. No. GTX135470, GeneTex), Flag (Cat. No. F1804, Sigma-Aldrich), and actin (Cat. No. NB600-501, Novus Biologicals) primary antibodies at 4 °C. After TSBT wash, the membranes were incubated for 1 h at room temperature with appropriate horseradish peroxidase (HRP)-conjugated secondary antibodies, and protein signals were visualized by a chemiluminescence ECL kit (HyCell International Co., Ltd.).

Flag-3CLpro-Overexpressed 293T Cells. Flag-3CLpro plasmid was purchased from SinoBiological (Cat. No. VG40594-NF). 293T control and 293T-3CLpro cells were seeded (3×10^4 cells/100 μL/well) and incubated in 96-well microplates and maintained at 37 °C in a humidified cell culture incubator with 5% CO_2. After 24 h, the supernatant of cells was refreshed with the virus-free infection media (with 2% FBS and 0.5% DMSO) in the presence of 3 μM Pentarlandir UPPTA for 2 h pretreatment. Subsequently, the supernatant was removed and refreshed with 50 μL of virus-containing media at a MOI of 1 and 3 μM Pentarlandir UPPTA. The total media volume was 100 μL, containing final concentrations of 0.5% DMSO and 2% FBS. After 48 h post infection at 33 °C, the supernatant of each well was subjected to RNA extraction using TRIzol reagent (Cat. No. 15596026, Thermo Fisher Scientific) and detected by a reverse transcription (RT)-PCR assay. The nucleoprotein gene of HCoV-OC43 was amplified using forward (5′-CGATGAGGCTATTCCGACTAGGT-3′) and reverse (5′-CCTTCCTGAGCCTTCAATATAGTAACC-3′) primers. Serial dilutions of HCoV-OC43 RNA with a known viral PFU were subjected to the same quantitative PCR and served to develop a standard curve to interpolate the viral counts of the drug candidate-treated cells.

Preparation of Vero E6 Cells. Vero E6 cells (ATCC No. CRL-1586) were maintained in Dulbecco's modified Eagle medium (DMEM, Cat. No. 11995040, Thermo Fisher Scientific) supplemented with 10% fetal bovine serum (FBS, Cat. No. 10437028, Thermo Fisher Scientific) in a humidified incubator at 37 °C with 5% CO_2 atmosphere. Cultured cells with 80−90% confluence were treated with 0.25% trypsin for cell detachment and passage. The treated cells were mixed with DMEM and centrifuged at 1000 rpm for 5 min for cell isolation and trypsin removal. After cell counting, Vero E6 cells were dispensed at a density of 10^4 cells/mL/well in a 96-well microplate and incubated for 24 h before experimentation. For the virucidal assay, the infection medium contained 2% FBS, as used in the literature.[23]

Cytotoxicity Assays. Vero E6 cells were seeded at a density of 10^4 cells/well onto 96-well plates and maintained at 37 °C and 5% CO_2 in a humidified cell culture incubator. After 24 h, the culture medium was removed, followed by the addition of 100 μL of DMEM with 2% FBS along with 10 μL of Pentarlandir UPPTA in the wells. The cells were then incubated for an additional 24 h. Subsequently, 100 μL of medium and 10 μL of Cell Counting Kit-8 solution (CCK8) solution (Cat. No. CK04-05, Dojindo Molecular Technologies, Inc.) were added to the cells with an incubation for 2 h, followed by the removal of the supernatant. The cell viability was determined following the formazan formation and

https://doi.org/10.1021/acsptsci.1c00264
ACS Pharmacol. Transl. Sci. XXXX, XXX, XXX−XXX

measured at the absorbance of 450 nm on a Sunrise microplate reader (Cat. No. INSTSUN-1, Tecan).

HCT8 cells were seeded at a density of 2×10^4 cells/well onto 96-well plates and maintained at 37 °C and 5% CO_2 in a humidified cell culture incubator. After 24 h, the culture medium was removed, followed by the addition of 10 μL of Pentarlandir UPPTA (0.39−800 μM) via serial dilution along with 100 μL of DMEM and 2% FBS in the wells. The cells were then incubated for an additional 24 h. Afterward, supernatant was removed and discarded, followed by addition of 110 μL of CCK-8 mixture in the cell culture and incubation for 2 h. The formazan concentrations, converted by water-soluble tetrazolium of the CCK-8 kit, in cultured wells were detected by a microplate reader (Tecan Sunrise, Männedorf, Switzerland) at the absorbance at 450 nm. The formazan concentrations were used as an indicator of cell viability.

SARS-CoV-2 Virucidal Assay. The SARS-CoV-2 virus was obtained from the Center for Disease Control, Taiwan. All virus-involved experiments were conducted in a Biosafety Level 3 (BSL3) laboratory at the Institute of Preventive Medicine, National Defense Medical Center, in Taiwan. The experimental procedures were modified from the literature.[23] Vero E6 cells were seeded (10^4 cells/100 μL/well) and incubated in 96-well microplates and maintained at 37 °C in a humidified cell culture incubator with 5% CO_2. After 24 h, the supernatant of Vero E6 cells was refreshed with the virus-free infection medium (with 2% FBS) containing different concentrations of Pentarlandir UPPTA. Subsequently, 100 μL of virus-containing medium with 2% FBS at MOI = 0.01 was added to each well of 96-well microplates to reach the indicated final concentrations of the drug candidate. The total medium volume was 200 μL, containing final concentrations of 1% DMSO and 2% FBS.

After 24 h of virus inoculation, the supernatant of each well was transferred and subjected to RNA extraction using a QIAamp Viral RNA mini kit (Cat. No. 52906, QIAGEN), and the cell layer of each well was subjected to RNA extraction using TRIzol reagent (Cat. No. 15596026, Thermo Fisher Scientific). Reverse transcription of cDNA was completed using a HiScript II Q RT SuperMix kit for qPCR (Cat. No. R223, Vazyme Biotech). The SARS-CoV-2 viral genome was quantified using two-step quantitative PCR on the StepOnePlus real-time PCR system (Applied Biosystems) with the SensiFASTTM SYBR Hi-ROX kit (Cat. No. BIO-92006, BIOLINE). The RNA-dependent RNA polymerase (RdRP) gene of SARS-CoV-2 was amplified using the forward (5′-GTGARATGGTCATGTGTGGCGG-3′) and reverse (5′-CARATGTTAAASACACTATTAGCATA-3′) primers.[24]

Serial dilutions of SARS-CoV-2 cDNA with a known viral PFU were subjected to the same quantitative PCR and served to develop a standard curve to interpolate the viral counts of the drug-candidate-treated cells. The SARS-CoV-2 virucidal activity was presented as percentage of inhibition and calculated using the following equation: inhibition (%) = [1 − (PFU_{sample}/PFU_{mean} of vehicle)] × 100%. The percentage of inhibition of the samples was plotted (Y axis) against logarithmic concentrations of the drug candidate (X axis). The concentration−inhibition plot was fitted with non-linear regression using an asymmetric (five-parameter) logistic dose−response curve.

HCoV-OC43 Virucidal Assay. The HCoV-OC43 virus was a gift from Professor Shin-Ru Shih, Chang Gang University, Taiwan. All HCoV-OC43-related experiments were conducted in a BSL2 laboratory at the Department of Pathology and Laboratory Medicine, Taipei Veterans General Hospital, Taiwan.

HCT8 cells were seeded (2×10^4 cells/100 μL/well) and incubated in 96-well microplates and maintained at 37 °C in a humidified cell culture incubator with 5% CO_2. After 24 h, the supernatant of the HCT8 cells was refreshed with the virus-free infection media (with 2% FBS and 0.5% DMSO) in the presence of increasing concentrations of Pentarlandir UPPTA for 2 h pre-treatment. Subsequently, the supernatant was removed and refreshed with 50 μL of virus-containing media at MOI = 0.05 and different concentrations of Pentarlandir UPPTA. The total media volume was 100 μL, containing final concentrations of 0.5% DMSO and 2% FBS. After 24 h post infection at 33 °C, the cell pellet of each well was subjected to RNA extraction using TRIzol reagent and detected by a reverse transcription (RT)-PCR assay.

The nucleoprotein gene of HCoV-OC43 was amplified using forward (5′-CGATGAGGCTATTCCGACTAGGT-3′) and reverse (5′-CCTTCCTGAGCCTTCAATATAGTAACC-3′) primers. Serial dilutions of HCoV-OC43 RNA with a known viral PFU were subjected to the same quantitative PCR and served to develop a standard curve to interpolate the viral counts of the drug-candidate-treated cells. The virucidal activity was presented as percentage of inhibition and calculated using the following equation: inhibition (%) = [1 − (PFU_{sample}/PFU_{mean} of vehicle)] × 100%. The percentage of inhibition of the samples was plotted (Y axis) against logarithmic concentrations of the drug candidate (X axis). The concentration−inhibition plot was fitted with non-linear regression using an asymmetric (five-parameter) logistic dose−response curve.

Pharmacokinetic Studies. Experimental procedures used in animal studies were approved by the Institutional Animal Care and Use Committee (IACUC) at SyneuRx International (Taiwan) Corp. Pentarlandir UPPTA was dissolved in ddH_2O, whereby the vehicle control group was administered. Grouping information for drug candidate-treated rats in the absorption studies is as follows: Group 1: fasting single dose, 1000 (mg/kg), 7 rats; Group 2: fasting single dose, 750 (mg/kg), 5 rats; Group 3: fasting single dose, 350 (mg/kg), 6 rats; Group 4: fasting 14-day repeated dose, 1000 (mg/kg), 6 rats; Group 5: fed single dose, 1000 (mg/kg), 5 rats. Groups 1−3 were fasted overnight; Group 4 was fasted 3 h every day before the administration of the drug candidate during the experiment period; and Group 5 received no fasting. Blood samples (∼500 μL) were collected from Groups 1 and 2 at pre-dosing (0 h) and 0.25, 0.5, 1, 2, 4, 6, 8, and 24 h post-dosing. In addition, blood samples were collected from Groups 3−5 at pre-dosing (0 h) and 1, 2, 4, 5, 6, 7, and 24 h post-dosing. The collected blood samples were transferred into tubes with 5 μL of heparin (5000 IU/mL) and centrifuged at 4000g for 10 min at 2−8 °C. The supernatant was transferred into new tubes and stored at −80 °C until analysis. Blood samples were subjected to tannase (167 U/g, E. Merck KGaA, Germany) hydrolysis to release free gallic acid prior to liquid chromatography/mass spectrometry (LC/MS) analysis (Shimadzu, LC/MS-2020, Japan), where the internal standard was 3,5-dihydroxybenzoic acid (Sigma-Aldrich, Germany).

For the determination of concentration in pulmonary tissues, rats were allocated into six groups. Groups A−C were given a single dose of 1000 mg/kg and fasted overnight, while Groups D−F were given a 14-day repeat dose of 1000

https://doi.org/10.1021/acsptsci.1c00264
ACS Pharmacol. Transl. Sci. XXXX, XXX, XXX−XXX

mg/kg and fasted 3 h every day before the administration of the drug candidate during the experimental period. Lung samples were collected from the animals at 4, 7, and 24 h after dosing. The pulmonary tissue samples from the six groups of animals (7−9 per group) were frozen rapidly in liquid nitrogen and stored at −80 °C until analysis. Upon the LC/MS analysis, the lung samples were subjected to tannase hydrolysis to release free gallic acid; 4-hydroxybenzoic acid was used as an internal standard.

Toxicology. This study followed the experimental procedures approved by the Institutional Animal Care and Use Committee (IACUC) at Level Biotechnology Inc. and was conducted under good laboratory practice (GLP) regulations. Pentarlandir UPPTA was dissolved in ddH_2O, whereby vehicle control group was administered. Grouping information for drug-treated rats in the 14-day repeat-dose toxicity study is described below. Fifteen rats were assigned to each group at dosage levels of 800, 1600, and 2000 mg/kg, where 10 animals were subjected to 14-day treatment, while the other 5 were given an additional 14-day recovery following drug treatment. Each rat was administered via oral gavage under a fasting condition, where rats were fasted 3 h before dosing and fed with food *ab libitum* 4 h post-dosing. The study monitored mortality/moribundity, body weight, food consumption, clinical observations, ophthalmologic examinations, vaginal smear, clinical pathology (including hematology, coagulation, serum chemistry, urinalysis, and urinary sediments examination), gross necropsy, and histopathology.

Statistical Analysis. Data collected are presented as mean ± SD, unless otherwise specified. The determination of IC_{50} was conducted using four logistic parameter functions from Prism. Student *t* tests were used for the 3CLpro overexpression and PK data analysis. A one-way ANOVA method that followed Dunnett's method was performed in the toxicology study.

AUTHOR INFORMATION

Corresponding Author

Guochuan Emil Tsai − *Department of Research and Development, SyneuRx International (Taiwan) Corp., New Taipei City 22175, Taiwan; UCLA School of Medicine, Los Angeles, California 90095, United States;* orcid.org/0000-0002-5124-3841; Email: tsaimdphd@ucla.edu

Authors

Po-Chang Shih − *Department of Research and Development, SyneuRx International (Taiwan) Corp., New Taipei City 22175, Taiwan;* orcid.org/0000-0002-6124-5090

Yi-Wen Mao − *Department of Research and Development, SyneuRx International (Taiwan) Corp., New Taipei City 22175, Taiwan*

Jhe-Wei Hu − *Department of Research and Development, SyneuRx International (Taiwan) Corp., New Taipei City 22175, Taiwan*

Han-Yi Hsieh − *Department of Research and Development, SyneuRx International (Taiwan) Corp., New Taipei City 22175, Taiwan*

Tsai-Miao Shih − *Department of Research and Development, SyneuRx International (Taiwan) Corp., New Taipei City 22175, Taiwan*

Lu-Ping Lu − *Department of Research and Development, SyneuRx International (Taiwan) Corp., New Taipei City 22175, Taiwan*

Wei-Hua Chang − *Department of Research and Development, SyneuRx International (Taiwan) Corp., New Taipei City 22175, Taiwan*

Chan-Hui Huang − *Department of Research and Development, SyneuRx International (Taiwan) Corp., New Taipei City 22175, Taiwan*

Chia-Hung Lin − *Department of Research and Development, SyneuRx International (Taiwan) Corp., New Taipei City 22175, Taiwan*

Chih-Hung Lin − *Department of Research and Development, SyneuRx International (Taiwan) Corp., New Taipei City 22175, Taiwan*

Peng Tan − *Department of Research and Development, SyneuRx International (Taiwan) Corp., New Taipei City 22175, Taiwan*

Ya-Ching Yang − *Department of Research and Development, SyneuRx International (Taiwan) Corp., New Taipei City 22175, Taiwan*

Ming-Hong Chien − *Department of Research and Development, SyneuRx International (Taiwan) Corp., New Taipei City 22175, Taiwan*

Chen-Che Su − *Department of Research and Development, SyneuRx International (Taiwan) Corp., New Taipei City 22175, Taiwan*

Cheng-Hsin Yeh − *Department of Research and Development, SyneuRx International (Taiwan) Corp., New Taipei City 22175, Taiwan*

Pei-Yun Chuang − *Department of Research and Development, SyneuRx International (Taiwan) Corp., New Taipei City 22175, Taiwan*

Tien-Lan Hsieh − *Department of Research and Development, SyneuRx International (Taiwan) Corp., New Taipei City 22175, Taiwan*

Ching-Cheng Wang − *Department of Research and Development, SyneuRx International (Taiwan) Corp., New Taipei City 22175, Taiwan*

Po-Shiuan Hsieh − *Institute of Physiology, National Defense Medical Center, Taipei City 11490, Taiwan; Department of Medical Research, Tri-Service General Hospital, Taipei City 114, Taiwan*

Teh-Ying Chou − *Department of Pathology and Laboratory Medicine, Taipei Veterans General Hospital, Taipei City 112, Taiwan; Institute of Clinical Medicine, National Yang-Ming Chiao Tung University, Taipei City 112304, Taiwan*

Complete contact information is available at: https://pubs.acs.org/10.1021/acsptsci.1c00264

Author Contributions

†P.-C.S., Y.-W.M., J.-W.H., H.-Y.H., T.-M.S., L.-P.L., W.-H.C., C.-H.H., and C.-H.L. contributed equally.

Funding

The study was sponsored by SyneuRx International (Taiwan) Corp.

Notes

Pentarlandir is protected by a patent in the U.S. (US11154531), and at the time of manuscript preparation, the patent application was pending in Taiwan and PCT (Patent Cooperation Treaty).

The authors declare the following competing financial interest(s): All authors, except for Po-Shiuan Hsieh and Teh-Ying Chou, are employees of SyneuRx International (Taiwan) Corp.

https://doi.org/10.1021/acsptsci.1c00264
ACS Pharmacol. Transl. Sci. XXXX, XXX, XXX−XXX

■ ACKNOWLEDGMENTS

We thank Professor Shin-Ru Shih (Chang Gung University, Taiwan) for her gift of the virus strains.

■ ABBREVIATIONS

3CLpro, 3-chymotrypsin-like protease; API, active pharmaceutical ingredient; $AUC_{0-t}/AUC_{0-\infty}$, area under the concentration−time curve from time 0 to the last sampling time or infinite time; Bis-Tris, bis(2-hydroxyethyl)amino-tris-(hydroxymethyl)methane; CC_{50}, 50% cytotoxicity concentration; COBALT, constraint-based alignment tool; CoV, coronavirus; C_{max}, maximum plasma concentration; Dabcyl, 4-(4-dimethylaminophenylazo)benzoic acid; ddH_2O, distilled, deionized water; DMEM, Dulbecco's modified Eagle medium; DTT, dithiothreitol; EC_{50}, 50% effective concentration; Edans, 5-[(2-aminoethyl)amino]naphthalene-1-sulfonic acid; EDTA, ethylenediaminetetraacetic acid; FBS, fetal bovine serum; GLP, good laboratory practice; HED, human equivalent dose; HPLC, high-performance liquid chromatography; IACUC, Institutional Animal Care and Use Committee; IC_{50}, 50% inhibition concentration; IP, investigational drug product; IPTG, isopropyl-β-D-1-thiogalactopyranoside; LB, Luria−Bertani; LC/MS, liquid chromatography/mass spectrometry; MOI, multiplicity of infection; NaCl, sodium chloride; NCBI, National Center for Biotechnology Information; NOAEL, no-observed-adverse-effect level; Nsp5, non-structural protein 5; Pentarlandir, ultrapure and potent tannic acids; PFU, plaque-forming unit; PK, pharmacokinetic; RT-PCR, reverse transcription polymerase chain reaction; SARS-CoV-2, severe acute respiratory syndrome coronavirus 2; $T_{1/2}$, half-life; T_{max}, time to reach C_{max}; Tris-HCl, tris(hydroxymethyl)aminomethane hydrochloride

■ REFERENCES

(1) Zhou, P.; Yang, X.-L.; Wang, X.-G.; Hu, B.; Zhang, L.; Zhang, W.; Si, H.-R.; Zhu, Y.; Li, B.; Huang, C.-L.; Chen, H.-D.; Chen, J.; Luo, Y.; Guo, H.; Jiang, R.; Liu, M. Q.; Chen, Y.; Shen, X. R.; Wang, X.; Zheng, X. S.; Zhao, K.; Chen, Q. J.; Deng, F.; Liu, L. L.; Yan, B.; Zhan, F. X.; Wang, Y. Y.; Xiao, G. F.; Shi, Z. L. A Pneumonia Outbreak Associated with a New Coronavirus of Probable Bat Origin. *Nature* **2020**, *579*, 270.

(2) The World Health Organization (WHO). Naming the Coronavirus Disease (COVID-19) and the Virus That Causes It. Feb 11, 2020. https://www.who.int/emergencies/diseases/novel-coronavirus-2019/technical-guidance/naming-the-coronavirus-disease-(covid-2019)-and-the-virus-that-causes-it.

(3) Vijgen, L.; Keyaerts, E.; Moës, E.; Thoelen, I.; Wollants, E.; Lemey, P.; Vandamme, A.-M.; Van Ranst, M. Complete Genomic Sequence of Human Coronavirus OC43: Molecular Clock Analysis Suggests a Relatively Recent Zoonotic Coronavirus Transmission Event. *J. Virol.* **2005**, *79*, 1595.

(4) Hamre, D.; Procknow, J. J. A New Virus Isolated from the Human Respiratory Tract. *Proc. Soc. Exp. Biol. Med.* **1966**, *121*, 190.

(5) Liu, D. X.; Liang, J. Q.; Fung, T. S. Human Coronavirus-229E, -OC43, -NL63, and -HKU1 (Coronaviridae). In *Encyclopedia of Virology*; Bamford, D. H., Zuckerman, M., Eds.; Elsevier, 2021; pp 428−440.

(6) Totura, A. L.; Bavari, S. Broad-Spectrum Coronavirus Antiviral Drug Discovery. *Expert Opinion on Drug Discovery* **2019**, *14*, 397.

(7) Wu, C.; Liu, Y.; Yang, Y.; Zhang, P.; Zhong, W.; Wang, Y.; Wang, Q.; Xu, Y.; Li, M.; Li, X.; Zheng, M.; Chen, L.; Li, H. Analysis of Therapeutic Targets for SARS-CoV-2 and Discovery of Potential Drugs by Computational Methods. *Acta Pharm. Sin. B* **2020**, *10*, 766.

(8) Yang, H.; Xie, W.; Xue, X.; Yang, K.; Ma, J.; Liang, W.; Zhao, Q.; Zhou, Z.; Pei, D.; Ziebuhr, J.; Hilgenfeld, R.; Yuen, K. Y.; Wong, L.; Gao, G.; Chen, S.; Chen, Z.; Ma, D.; Bartlam, M.; Rao, Z. Design of Wide-Spectrum Inhibitors Targeting Coronavirus Main Proteases. *PLoS Biol.* **2005**, *3*, e324.

(9) Sawicki, S. G.; Sawicki, D. L.; Siddell, S. G. A Contemporary View of Coronavirus Transcription. *J. Virol.* **2007**, *81*, 20.

(10) Larsen, J. R.; Martin, M. R.; Martin, J. D.; Kuhn, P.; Hicks, J. B. Modeling the Onset of Symptoms of COVID-19. *Front. Public Health* **2020**, *8*, 473.

(11) Liu, P.; Liu, H.; Sun, Q.; Liang, H.; Li, C.; Deng, X.; Liu, Y.; Lai, L. Potent Inhibitors of SARS-CoV-2 3C-like Protease Derived from N-Substituted Isatin Compounds. *Eur. J. Med. Chem.* **2020**, *206*, 112702.

(12) Chen, C. N.; Lin, C. P. C.; Huang, K. K.; Chen, W. C.; Hsieh, H. P.; Liang, P. H.; Hsu, J. T. A. Inhibition of SARS-CoV 3C-like Protease Activity by Theaflavin-3,3′- Digallate (TF3). *Evidence-based Complement. Altern. Med.* **2005**, *2*, 209.

(13) Guinard, J. -X; Pangborn, R. M.; Lewis, M. J. Preliminary Studies on Acidity-astringency Interactions in Model Solutions and Wines. *J. Sci. Food Agric.* **1986**, *37*, 811.

(14) Belleau, G.; Dadic, M. Determination of Tannic Acid in Beer by High Performance Liquid Chromatography. *Am. Soc. Brew. Chem. J.* **1979**, *37* (4), 175−179.

(15) Gülçin, I.; Huyut, Z.; Elmastaş, M.; Aboul-Enein, H. Y. Radical Scavenging and Antioxidant Activity of Tannic Acid. *Arab. J. Chem.* **2010**, *3*, 43.

(16) Andrade, R. G.; Dalvi, L. T.; Silva, J. M. C.; Lopes, G. K. B.; Alonso, A.; Hermes-Lima, M. The Antioxidant Effect of Tannic Acid on the in Vitro Copper-Mediated Formation of Free Radicals. *Arch. Biochem. Biophys.* **2005**, *437*, 016.

(17) Tikoo, K.; Sane, M. S.; Gupta, C. Tannic Acid Ameliorates Doxorubicin-Induced Cardiotoxicity and Potentiates Its Anti-Cancer Activity: Potential Role of Tannins in Cancer Chemotherapy. *Toxicol. Appl. Pharmacol.* **2011**, *251*, 191.

(18) Chung, K. T.; Lu, Z.; Chou, M. W. Mechanism of Inhibition of Tannic Acid and Related Compounds on the Growth of Intestinal Bacteria. *Food Chem. Toxicol.* **1998**, *36*, 1053.

(19) Lee, J. H.; Park, J. H.; Cho, H. S.; Joo, S. W.; Cho, M. H.; Lee, J. Anti-Biofilm Activities of Quercetin and Tannic Acid against Staphylococcus Aureus. *Biofouling* **2013**, *29*, 491.

(20) Carson, R. S.; Frisch, A. W. The Inactivation of Influenza Viruses by Tannic Acid and Related Compounds. *J. Bacteriol.* **1953**, *66*, 572.

(21) Chen, Y. W.; Yiu, C.-P. B.; Wong, K.-Y. Prediction of the SARS-CoV-2 (2019-NCoV) 3C-like Protease (3CLpro) Structure: Virtual Screening Reveals Velpatasvir, Ledipasvir, and Other Drug Repurposing Candidates. *F1000Research* **2020**, *9*, 129.

(22) Kuo, C. J.; Chi, Y. H.; Hsu, J. T. A.; Liang, P. H. Characterization of SARS Main Protease and Inhibitor Assay Using a Fluorogenic Substrate. *Biochem. Biophys. Res. Commun.* **2004**, *318*, 862.

(23) Choy, K. T.; Wong, A. Y. L.; Kaewpreedee, P.; Sia, S. F.; Chen, D.; Hui, K. P. Y.; Chu, D. K. W.; Chan, M. C. W.; Cheung, P. P. H.; Huang, X.; Peiris, M.; Yen, H. L. Remdesivir, Lopinavir, Emetine, and Homoharringtonine Inhibit SARS-CoV-2 Replication in Vitro. *Antiviral Res.* **2020**, *178*, 104786.

(24) Corman, V. M.; Landt, O.; Kaiser, M.; Molenkamp, R.; Meijer, A.; Chu, D. K. W.; Bleicker, T.; Brünink, S.; Schneider, J.; Schmidt, M. L.; Mulders, D. G. J. C.; Haagmans, B. L.; Van Der Veer, B.; Van Den Brink, S.; Wijsman, L.; Goderski, G.; Romette, J. L.; Ellis, J.; Zambon, M.; Peiris, M.; Goossens, H.; Reusken, C.; Koopmans, M. P. G.; Drosten, C. Detection of 2019 Novel Coronavirus (2019-NCoV) by Real-Time RT-PCR. *Eurosurveillance* **2020**, DOI: 10.2807/1560-7917.ES.2020.25.3.2000045.

(25) Wang, S.-C.; Chen, Y.; Wang, Y.-C.; Wang, W.-J.; Yang, C.-S.; Tsai, C.-L.; Hou, M.-H.; Chen, H.-F.; Shen, Y.-C.; Hung, M.-C. Tannic Acid Suppresses SARS-CoV-2 as a Dual Inhibitor of the Viral Main Protease and the Cellular TMPRSS2 Protease. *Am. J. Cancer Res.* **2020**, *10*, 4538−4546.

https://doi.org/10.1021/acsptsci.1c00264
ACS Pharmacol. Transl. Sci. XXXX, XXX, XXX−XXX

(26) Vatansever, E. C.; Yang, K.; Kratch, K. C.; Drelich, A.; Cho, C.-C.; Mellot, D. M.; Xu, S.; Tseng, C.-T. K.; Liu, W. R. Targeting the SARS-CoV-2 Main Protease to Repurpose Drugs for COVID-19. *bioRxiv Preprint* **2020**, 112235.
(27) Janower, M. L.; Robbins, L. L.; Tomchik, F. S.; Weylman, W. T. Tannic Acid and the Barium Enema. *Radiology* **1965**, *85* (5), 887−894.
(28) Lia, J.; Lin, C.; Zhou, X.; Zhong, F.; Zeng, P.; Yang, Y.; Zhang, Y.; Yu, B.; Fan, X.; McCormick, P. J.; Fu, R.; Fu, Y.; Jiang, H.; Zhang, J. Structural basis of main proteases of coronavirus bound to drug candidate PF-07321332. *bioRxiv Preprint* **2021**, 467529.

https://doi.org/10.1021/acsptsci.1c00264
ACS Pharmacol. Transl. Sci. XXXX, XXX, XXX−XXX